IMPROVED PMSM FOR WIND TURBINE APPLICATIONS WITH MULTIPLE HIGH-SPEED GENERATORS

Invited paper from the International Conference on Optimization of Electrical and Electronic Equipment (OPTIM) [24], May 22–24, 2014, Brasov

Cristian ANDREI **Tobias KAUDER** **Jan KARTHAUS**
Marco HOMBITZER **Rüdiger APPUNN** **Kay HAMEYER**
Institute of Electrical Machines, RWTH Aachen University, Schinkelstraße 4, 52062 Aachen, Germany,
Tel: +49 241 80 97643, Fax: +49 241 80 92270, Email: cristian.andrei@iem.rwth-aachen.de

Abstract: *Wind turbines (WTs) are energy conversion systems with a very complex electromechanical structure, consisting of highly interconnected subsystems, which are constantly exposed to dynamic electrical and mechanical stress. In order to improve their technical and economic efficiency, new alternative drive train concepts are being sought. This paper proposes a WT drive train with multiple high-speed generators. Different electrical machines are investigated analytically and the permanent magnet synchronous machine with V-shaped internal magnets (VI-PMSM) is chosen as the most suited topology for this application. A simple MATLAB Simulink model is developed to validate the proposed WT configuration in terms of efficiency gain. Furthermore, the operational behavior of the VI-PMSM is improved by means of sinusoidal rotor field poles.*

Key words: *Wind power generation, Electric machines, Permanent magnet machines, Rotors.*

1. Introduction and Motivation

With regard to the rapidly increasing lack of conventional fossil-fuel based energy sources, the public interest around the world has been shifted in the last decades towards renewable and more reliable energy resources. The wind energy sector is no exception from this trend. In fact, wind energy is one of the most important players in today's world energy market. As it can be seen in Figure 1, since 1996 there has been a constant growth of the yearly installed global wind energy capacity of about 26 %, which led to a total installed capacity of more than 280 GW in 2012 [1].

This growth rate also led to major technical improvements regarding the applied WT concepts. In the early 2000s a change of concept took place, from the robust and inexpensive, yet electrically rigid WT with squirrel cage induction generators (SCIG) to the more grid-friendly variable speed solutions. This change was based on both technical and economic grounds. WTs were still a large capital expenditure at that time, despite many grants and subsidies provided by most governments for the development of the wind industry. The revenue from wind generated electricity had to be increased, which in turn meant that more installed electrical power per turbine was required. Therefore, variable speed concepts became essential [2].

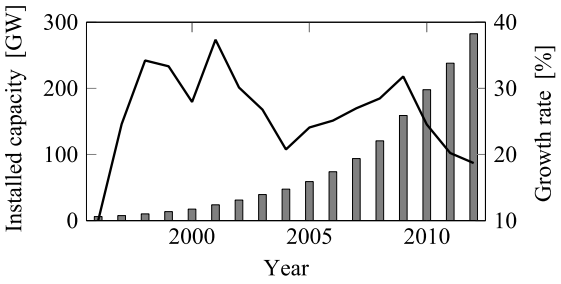

Fig. 1. Global cumulative installed wind capacity.

The following four variable speed WT concepts represent the state-of-the-art and dominate today's wind energy market:

- The WT concept with a three-stage gearbox and a doubly fed induction generator (DFIG),
- the gearless WT with an electrically excited synchronous generator (DD EESG),
- the gearless WT with a synchronous generator with permanent magnet (PM) excitation (DD PMSG) and
- the WT concept with an one- or two-stage gearbox and a PM excited synchronous generator (2G PMSG).

Despite their technological maturity and market domination, these concepts still display some major disadvantages and drawbacks, especially regarding downtime and availability, with the gearbox, generator and electrical system having the highest components failure rates. Thus, according to different statistical reliability studies performed in Germany, Sweden and Finland, downtimes of up to 152 hours per year have been determined [3–7].

The main disadvantage of the DFIG concept for instance is the expensive and fault-prone three-stage gearbox, which is mandatory for this concept, since the generator is directly connected to the grid and its speed (1200–1800 min^{-1}) is much higher than that of the rotor (12–15 min^{-1}). During voltage dips a so-called crowbar system can be connected in the rotor circuit of the DFIG, in order to short-circuit it and avoid the induction of high currents in the frequency converter, which leads to high shock loads in the gearbox, especially after the fault clearance [2, 8, 9].

The direct-drive gearless DD EESG and PMSG concepts do not have the disadvantage of a high-maintenance gearbox; however the generators used here are bulky low-speed high torque electrical machines with diameters of several meters. This results in increased production and investment costs and higher weights, not only for the nacelles, but also for the towers. Also, full-scale frequency converters are used in order to fully decouple the generators from the grid, which further adds to the cost and weight of these concepts [2, 10–13].

The separate controllable rectifier in the rotor circuit of the DD EESG, needed to provide the excitation, is also the cause of additional losses. On the other hand, the PMs used in the DD PMSG concept are a constant financial insecurity, due to the price fluctuations over the last years. When regarding the PM mass used in WTs (about one ton per megawatt), the influence of the PMs on the total investment cannot be underestimated [10, 11, 14].

The 2G PMSG shows some advantages when compared to the direct-drive concepts, in that the drive train is more compact, because of the integration of the one- or two-stage gearbox and the generator. However, higher maintenance and a somewhat increased cost factor—due to the existence of the gearbox and the use of PMs—are still an issue with this concept [12, 13, 15].

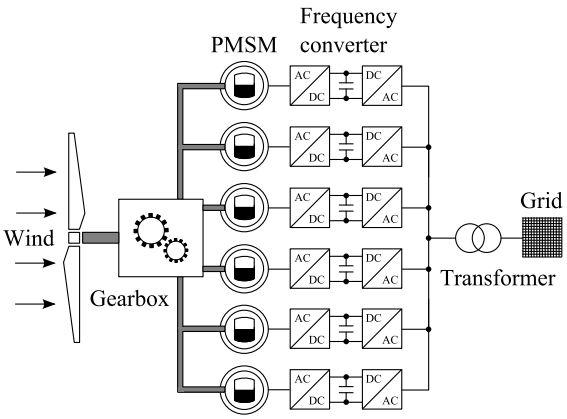

Fig. 2. Schematic diagram of a WT with six high-speed generators.

Based on the aforementioned drawbacks of the four conventional concepts, a series of requirements can be defined, which alternative drive trains have to fulfill, in order to assure the technical and economic improvement of future WTs:

- High power density
- Increased system efficiency
- Reduced weight and size
- Low investment and production costs
- Reduced maintenance and low downtimes

To meet these requirements an alternative WT drive train with multiple high-speed generators is proposed in this paper. A schematic diagram of the proposed concept is shown in Figure 2.

This drive train combines the advantages of the WT concept with multiple generators [16, 17] with those of the high-speed application of electrical machines, which is already used in the automotive and off-highway machines industry: significant material and cost reduction, high availability and increased energy efficiency. The gearbox used for this concept needs a fourth gear stage, when compared to the more conventional configurations, since the targeted speed is 5000 min^{-1} (much higher than that of similar concepts [3]) and thus a transmission ratio of up to 500 is needed. This fourth gear stage can lead to additional losses or downtimes. However, these drawbacks can be compensated through an optimized operational strategy, since a part of the drives can be shut down in partial load. The concept shown in Figure 2 displays six generators, but versions with four or eight generators are also conceivable.

The targeted higher speed of the generators results in an increased power density, which brings a considerable weight and size reduction of the drive train. This further leads to a significant saving of magnetic active material (electrical steel, copper and PMs) and thus to a decrease of the investment costs. The design with multiple identically constructed generators means that more identical parts will be available. At the same time, these parts are smaller and lighter than the parts of conventional turbines, due to the power split configuration. This results in an increased economic efficiency in the production and the reduction of downtimes. First considerations regarding a similar concept of a 3 MW WT with

Table 1. Modeling characteristics.

WT characteristics		
Rated power	P_{WT}	6 MW
Rated speed	n_{WT}	11.11 min^{-1}
Rated wind	v_N	13 $\frac{\text{m}}{\text{s}}$
Cut-in wind	$v_{cut\text{-}in}$	3 $\frac{\text{m}}{\text{s}}$
Cut-out wind	$v_{cut\text{-}out}$	25 $\frac{\text{m}}{\text{s}}$
Rotor diameter	D_{rot}	126 m
Hub height	h_{hub}	100 m
Power coeff.	$c_{P,max}$	0.467
Tip speed ratio	$\lambda_{WT,opt}$	7.6
Air density	ρ_{air}	1.225 $\frac{\text{kg}}{\text{m}^3}$

Machine parameters				
		SCIM	EESM	PMSM
Rated power	P_N	1 MW	1 MW	1 MW
Rated voltage	U_N	690 V	690 V	690 V
Rated speed	n_N	5000 min^{-1}	5000 min^{-1}	5000 min^{-1}
Phases	m	3	3	3
Pole pairs	p	4	4	4
Power factor	$\cos\varphi$	0.875	0.8	0.8
Efficiency	η	0.95	0.96	0.97
Esson coeff.	C	4.25 $\frac{\text{kW}\cdot\text{min}}{\text{m}^3}$	5.5 $\frac{\text{kW}\cdot\text{min}}{\text{m}^3}$	5.5 $\frac{\text{kW}\cdot\text{min}}{\text{m}^3}$
Relative length	λ	4	2.5	2.5
Air gap length	δ	0.6 mm	2 mm	2 mm
Air gap field	B_m	0.8 T	1.2 T	1.189 T
PM height	h_{PM}	–	–	10 mm

four generators show that the overall downtimes of the system can be reduced from 152 (DFIG) to 138 hours per year. Also, a maintenance costs reduction of about 20000 EUR per year was determined, when compared for instance to the conventional gearless concepts. Furthermore, for such configurations some of the generators can be shut down in partial load operation and the distribution of the wind energy can be optimized according to efficiency. A certain redundancy of the system is therefore given as well, since energy will always be produced, even in case of a malfunction of one generator.

The purpose of this paper is to illustrate some of the advantages of this alternative WT drive train concept. Section 2 presents the studied electrical machine topologies ensuing from analytical calculations and the choosing of the VI-PMSM as the most suited topology for this application. In section 3 the drive train model in MATLAB Simulink is outlined. The VI-PMSM used here is implemented based on the efficiency map of a reference machine. Finally, a method to reduce cogging torque and undesired harmonics and thus to improve the operational behavior of the used VI-PMSM configuration is shown in section 4.

2. Studied Electrical Machines

In order to choose the most suited electrical machine to be used as a generator in the proposed drive train, three topologies are regarded in this section: the squirrel cage induction machine (SCIM), the electrically excited synchronous machine (EESM) and the synchronous machine with PM excitation (PMSM). First, the technical requirements and constraints for the WT and for the investigated machines are defined and summarized. Subsequently, the three machine topologies are designed based on analytical formulas and compared to one another regarding their rated efficiency and power density.

A. Technical Requirements

For the modeling of the drive train with multiple high-speed generators a large onshore variable speed, pitch-controlled WT with 6 MW rated power and a rotor diameter of 126 m is presumed. Further characteristics of this turbine are given in Table 1.

Before starting with the analytical design, a series of parameters and modeling characteristics for the three electrical machines have to be assumed (see Table 1), like the rated voltage, the number of pole pairs or the power factor. These parameters are defined based on specifications in [18] and rely mostly on experience. At the same time, thermal limits and saturation of the magnetic active material are taken into account.

B. Analytical Design

In this section, starting from the rated values, a SCIM, an EESM and a PMSM are designed analytically, according to the assumed parameters in Table 1. Subsequently, the calculated efficiencies and power densities allow a comparison of the discussed machines.

The main dimensions of the machines describe the basic geometry, like diameter or stack length, which are then required for the detailed winding layout.

When choosing the number of pole pairs for the machines, the switching frequency of the converters—in this case 3 kHz—has to be taken into account. Usually, the frequency of the machine should be about ten times lower than that of the

converter. Therefore, a number of p=4 pole pairs is chosen for now, which results in a frequency of f_N=333.33 Hz.

Dependent on the assumed rated values for voltage, efficiency and power factor, the induced voltage U_{ind}, input power P_{mech} and rated current I_N can be determined. These parameters characterize the behavior of the machines and are required for the subsequent analytical calculations. To calculate the bore diameter D_S, the ideal active stack length l_i and the pole pitch τ_p of the machines, an adequate Esson coefficient C has to be chosen [18]:

$$D_S = \sqrt[3]{\frac{2 \cdot P_{mech} \cdot p}{n_N \cdot C \cdot \pi \cdot \lambda}} \tag{1}$$

The pole pitch allows the determination of the number of slots per pole and phase q_S and has an influence on the magnetic flux in the air gap Φ_δ, which is calculated based on the assumed mean value of the air gap magnetic field B_m. Assuming the magnetic flux in the air gap corresponds to the main flux Φ_h, the number of turns w_S can be calculated.

Regarding the rotor, the slot geometry of the SCIM is determined by calculating the current in the rings I_{ring} and the bars I_{bar} of the rotor cage [18]. The slot geometry of the EESM is given by the excitation current I_f [18], while the slot geometry for the PMSM is dependent on the height of the PMs. In this case, for the basic analytic calculation implemented here, a rotor with surface mounted PMs is chosen.

The design of the windings and the machine geometry allows an evaluation of the copper and the iron losses of the machines. After calculating the resistances of the stator and rotor windings, the copper losses can be determined by

$$P_{losses,Cu} = m \cdot R \cdot I^2 \tag{2}$$

Table 2. Results of the analytical design.

		SCIM	EESM	PMSM
Outer diameter	D_{out}	416.9 mm	518.2 mm	474.1 mm
Total length	l_{tot}	657.6 mm	535.8 mm	649.1 mm
Volume	V	0.0897 m^3	0.113 m^3	0.115 m^3
Power density	P_ρ	11.15 $\frac{\text{MW}}{\text{m}^3}$	8.85 $\frac{\text{MW}}{\text{m}^3}$	8.69 $\frac{\text{MW}}{\text{m}^3}$
Efficiency	η	0.9542	0.9773	0.9731

An appropriate approach for the estimation of the iron losses, dependent on the specific iron mass m_{Fe}, the peak value of the magnetic field $\hat{B}$ and the frequency f, is given by the IEM-Formula described in [19], where the material dependent coefficients a_1–a_5 are determined by measurements:

$$P_{losses,Fe} = m_{Fe} \cdot \left[a_1 \cdot \hat{B}^2 \cdot f + a_2 \cdot \hat{B}^2 \cdot f^2 \cdot \left(1 + a_3 \cdot \hat{B}^{a_4}\right) + a_5 \cdot \hat{B}^{1.5} \cdot f^{1.5} \right] \tag{3}$$

In addition to the copper and iron losses, it is required to estimate the eddy current losses which occur in the PMs of the PMSM. The effects and an analytic estimation of these eddy currents are described in [20]. Only the effects caused by spatial stator current harmonics are considered, because the estimation of the eddy current losses due to time harmonics of the stator current or stator slotting does not result in proper values [21].

Finally, mechanical losses caused by friction in the bearing and air can be accounted for by [18]:

$$P_{losses,mech} = k_{fr} \cdot D_R \cdot \left(l_i + 0.8^3 \cdot 0.6 \cdot \tau_p\right) \cdot v_{circ}^2 \tag{4}$$

where k_{fr} represents an empirical friction coefficient, dependent on the used cooling system and v_{circ} is the peripheral speed on the rotor surface, which can be determined based on the rotational speed and the machines rotor diameter D_R. Since the cooling medium is not regarded at this point in the design, a worst-case approximation is eventually used for the calculation of the mechanical losses:

$$P_{losses,mech} = 0.01 \cdot P_{mech} \tag{5}$$

The calculated losses and geometry of the investigated machines yield their efficiencies and power densities. Herewith a comparison can be done and the most suited topology can be chosen. The efficiencies and power densities, as well as other resulting parameters are summarized in Table 2.

The SCIM displays the highest power density, while the EESM has the highest efficiency, although the difference is rather small when compared to the PMSM. For the PMSM, the eddy current losses in the surface mounted PMs are relatively high and can not be sufficiently accounted for. However, it is expected that the use of V-shaped internal magnets (VI-PMSM) would lead to a much higher efficiency for this machine [22]. For this reason the VI-PMSM is chosen for the following investigations.

3. Model of the WT Concept with Multiple High-speed Generators

In order to validate the efficiency improvement of a WT concept with multiple high-speed generators as opposed to other conventional concepts, a simple MATLAB Simulink model is introduced. This model has the same structure as presented schematically in Figure 2 and it consists of a wind calculation block, a gearbox unit block with an appropriate power split algorithm and, as previously mentioned, six identical generator blocks. These blocks are described briefly in the following sections.

A. Wind Model

The wind model transforms the wind energy depending on the wind speed into an input wind power and a turbine speed. Based on an existing map of the power coefficient for a 6 MW wind turbine—where the power coefficient is given as a function of the tip speed ratio and different pitch angles via look-up tables—a pitch control is designed. For an optimal pitch angle of ϑ_{opt}=0°, the optimal tip speed ratio λ_{opt} and maximum power coefficient $c_{P,max}$ given in Table 1 are reached. The input wind power can then be calculated as [10, 11]:

$$P_{wind,in} = \frac{1}{2} \cdot \rho_{air} \cdot \pi \cdot \left(\frac{D_{rot}}{2} \right)^2 \cdot v_{wind}^3 \cdot c_P(\vartheta, \lambda) \qquad (6)$$

B. Gearbox Model

The gearbox unit block consists of a simple transformation of the turbine speed into the input speed for the generators, where a transmission ratio of 450 is assumed. The speed of the six generators is identical at all times, which means that only the input torque coming from the turbine is divided among the generators. As it will be shown in the following, this power split yields an increase of the WT system efficiency at partial load, if the torque is divided unsymmetrically among the six generators. In order to avoid the underutilization of the electrical machines and further increase the efficiency of the system, the rated speed of the generators is set to be reached earlier then the rated power, at about 10 $\frac{\text{m}}{\text{s}}$ instead of 13 $\frac{\text{m}}{\text{s}}$. This ensures an operation of the generators closer to their rated point, for a wider wind speed range.

C. Generator Model

The main characteristics of the reference VI-PMSM used in this model are summarized in Table 3 and the geometry is illustrated in Figure 3. The efficiency map is shown in Figure 4.

Table 3. Characteristics of the reference VI-PMSM.

General data		
Rated power	P_N	1 MW
Rated voltage	U_N	690 V
Rated speed	n_N	5000 min^{-1}
Active length	l_i	480 mm
Stator		
Outer radius	$r_{S,out}$	240 mm
Yoke height	h_j	34 mm
Tooth width	b_t	20.4 mm
Slot height	h_s	53.6 mm
Air gap	δ	2.4 mm
No. of slots	n	36
Rotor		
Outer radius	$r_{R,out}$	150 mm
Inner radius	$r_{R,in}$	70 mm
PM angle	α_{PM}	70 °
PM height	h_{PM}	10 mm
Pole coverage	α_i	0.7
Pole pairs	p	3

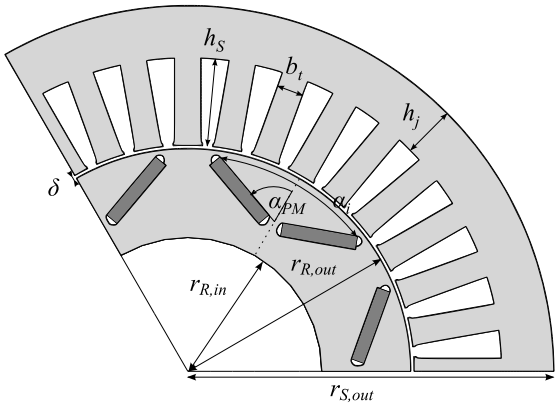

Fig. 3. 120° geometry model of the reference VI-PMSM.

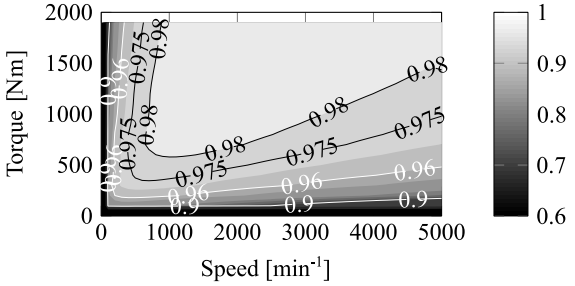

Fig. 4. Efficiency map of the reference VI-PMSM.

As previously stated, the six identical generators are implemented based on this efficiency map. An already existent model of such a topology was scaled up for the application as a 1 MW WT generator. It must be noted, that the number of pole pairs chosen here is smaller when compared to that of the design in section 2, in order to further increase the difference between the frequency of the machine and that of the converter.

D. WT System Model

Next to the advantages of redundancy and cost reduction due to the drive train construction with multiple high-speed generators, this concept also brings an efficiency increase of the WT system at partial load. For this purpose, the input torque has to be divided unsymmetrically among the generators, as previously described. Figure 5 shows that indeed an efficiency gain of almost 6 % can be reached in comparison to a symmetrical split of the input power.

4. VI-PMSM with Improved Rotor Pole Geometry

As previously mentioned, one other aim of this paper is the improvement of the operational behavior of the VI-PMSM, whose reference design was implemented as a generator in the proposed WT concept and described in section 3. For this purpose, sinusoidal rotor field poles are investigated. The minimization of the higher harmonics in the air gap and of the cogging torque, as well as the increase of the machines efficiency are the main goals of this investigation.

A. VI-PMSM with Sinusoidal Rotor Field Poles

According to [23], a sinusoidal rotor field is produced by the following relation for the air gap δ:

$$\delta(\beta) = \frac{\delta_d}{\cos\left(\frac{\pi}{\tau_p}\cdot\beta\right)} \tag{7}$$

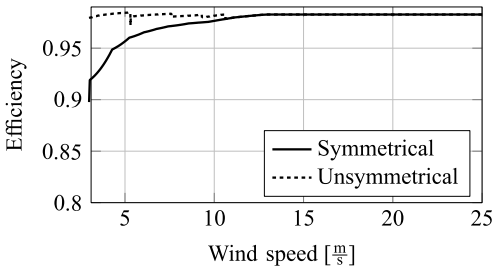

Fig. 5. Symmetrical vs. unsymmetrical power split.

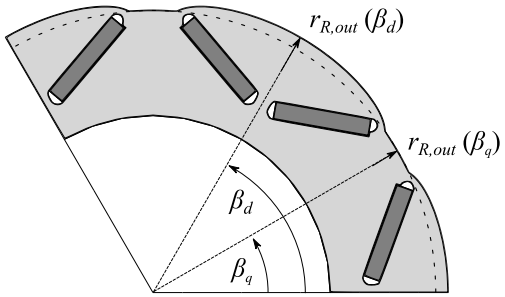

Fig. 6. 120° geometry model of the VI-PMSM with sinusoidal rotor field poles for $\frac{\delta_q}{\delta_d}$=4.

where τ_p is the pole pitch and β defines the angular position on the rotor. The shape of the rotor is given by:

$$r_{R,out}(\beta) = r_{S,in}\text{-}\delta(\beta) \tag{8}$$

It is obvious that the minimal air gap $\delta_{min}(\beta_d)$ is located in the *d*-axis of the machine and the maximal air gap $\delta_{max}(\beta_q)$ in the *q*-axis. To achieve different rotor pole shapes, the maximal air gap has to be limited. Equation 7 defines the air gap on the circumference of the rotor, as long as the definition of δ_{max} is not exceeded. Figure 6 shows an example of a new rotor shape given by equations 7 and 8.

The design parameter $\frac{\delta_q}{\delta_d}$ describes one specific rotor shape and therefore different rotor shapes can be compared based on this ratio:

$$\frac{\delta_q}{\delta_d} = \frac{\delta_{max}}{\delta_{min}} \tag{9}$$

B. Structural Analysis

The centrifugal forces, which occur in the rotor material, can have an undesired effect especially on the iron surrounding the PMs and need to be limited. Therefore, the mechanical stress on the side and central bridges of the rotor poles has to be investigated. These bridges are defined by the position of the PMs inside the rotor. The shortest distance from a PM to the rotor contour is defined as a side bridge. The distance between two PMs of one rotor pole is called the central bridge.

To lower the resulting centrifugal forces, the PM can be positioned deeper in the rotor. The trade-off between leakage flux and resulting centrifugal forces defines the width of the bridges. Figure 7 illustrates the mechanical stress for an exemplary case of the air gap ratio.

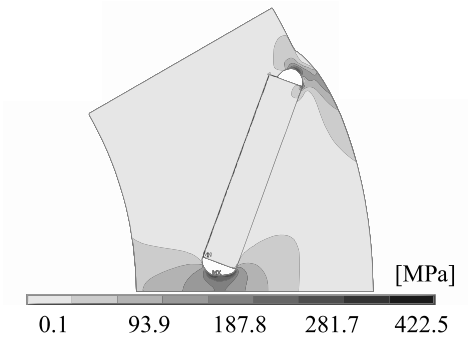

Fig. 7. Centrifugal force simulation for $\frac{\delta_q}{\delta_d}$=4.

C. No-Load Simulation

To analyze the behavior of different rotor pole shapes, a no-load simulation is first applied and different rotor shapes are compared to one another. The air gap ratio $\frac{\delta_q}{\delta_d}$ is varied from 1 to 10. Figure 8a shows that even a doubling of the air gap in the *q*-axis yields a minimization of the cogging torque of almost 30 Nm (from ± 35 to ± 6 Nm). This can also be seen in the fast Fourier transform (FFT) of the cogging torque in Figure 8b.

At the same time, the total harmonic distortion factor (THD) of the induced voltage in no-load operation decreases with an increasing air gap in *q*-axis. This is illustrated in Figure 9, where the voltages are simulated for a number of turns w=1 and are thus independent of this factor.

D. Rated Operation Point

For the computation of the torque at rated operation, a fixed current density of J=5.5 $\frac{\text{A}}{\text{mm}^2}$ is applied in the coils of the VI-PMSM with the different rotor designs. Because of the increased air gap in the *q*-axis of the machine, the total torque is reduced with increasing air gap ratio $\frac{\delta_q}{\delta_d}$. This is due to the reduction in reluctance torque, which stems from the magnetic anisotropy between the *q*- and the *d*-axis of the machine. With increasing air gap ratio, the magnetic flux paths must overcome more air in the *q*-axis than for the reference machine, which yields a matching of the inductances in the two axes. For inductances of the VI-PMSM design with sinusoidal rotor field poles it can therefore be stated that $L_q \xrightarrow{\delta_q \uparrow} L_d$, rather than $L_q > L_d$, as it is the case for the original design. The torque loss for different air gap ratios is illustrated in Table 4.

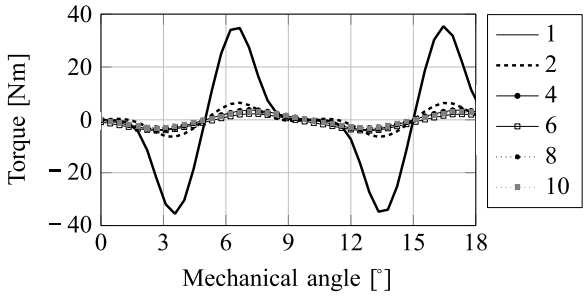

(a) Torque characteristics

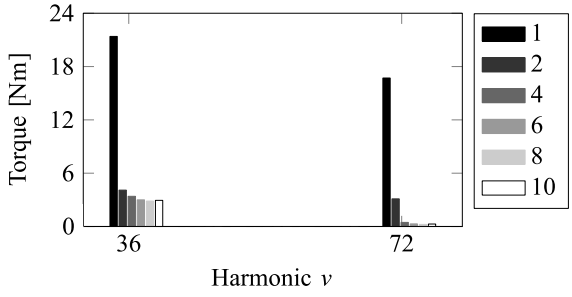

(b) FFT

Fig. 8. Cogging torque as a function of $\frac{\delta_q}{\delta_d}$.

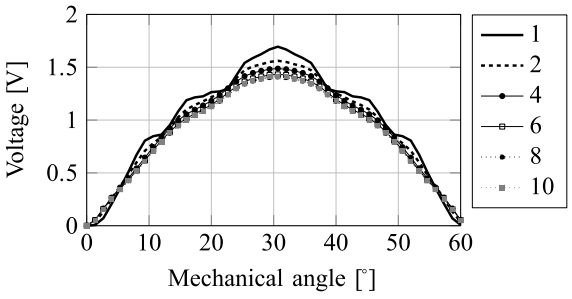

(a) Voltage characteristics

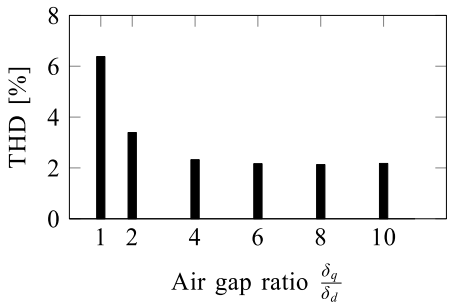

(b) THD

Fig. 9. Induced phase-to-phase voltage as a function of $\frac{\delta_q}{\delta_d}$.

Table 4. Maximum torque for different $\frac{\delta_q}{\delta_d}$.

$\frac{\delta_q}{\delta_d}$	T_{max}	
	[Nm]	[%]
1	1980	100
2	1670	84.3
4	1540	77.8
6	1490	75.3
8	1460	73.7
10	1460	73.7

E. Characteristic Diagrams

In order to conclude the investigation on the improvements brought by sinusoidal rotor field poles, a final comparison of the reference model and an adapted geometry is performed in this section, based on characteristics diagrams of the losses and efficiencies for the two machine topologies.

The previous simulations performed for the rated torque and also for different other operation points have indicated a decrease of the reluctance torque of the VI-PMSM with sinusoidal field poles and therefore of its total torque as well.

The machine has to be up scaled so that it delivers the same total torque for the same current as in the case of the reference design. For the VI-PMSM with an air gap ratio of $\frac{\delta_q}{\delta_d}$=4 the active length of the machine is increased to 620 mm, as opposed to 480 mm for the reference model. This corresponds to a machine growth of roughly 30 %, which means that the adapted design is heavier and has a lower power and torque density when directly compared to the original machine. Also, more PMs will be needed, which further adds to the cost factor. However, for smaller air gap ratios the size increase will most likely be less than 30 %, since more reluctance torque is delivered in these cases.

Figures 10a and 10b show the difference between the reference model and the design with $\frac{\delta_q}{\delta_d}$=4, regarding their copper and iron losses. The adapted geometry has slightly more copper losses than the reference machine (3 kW as opposed to 2.5 kW for the rated operation point), due to the increased overall length and therefore the increased copper windings mass and resistance. However, the design shows a significant reduction of the iron losses. This is most likely the outcome of the decrease in higher harmonics in the air gap.

For the rated operation point for instance, the difference in the iron losses is 3 kW (11.1 kW for the reference machine and only 8.1 kW for the design with sinusoidal rotor field poles), which leads to an improvement of 27 % regarding this aspect.

Furthermore, it must be noted that in the case of the VI-PMSM with adapted rotor geometry, the iron losses correspond to an active length of 620 mm. This means that despite the 30 % increase in iron material, the design with sinusoidal rotor field poles yields less iron losses than the original design. In total, for the machine with adapted geometry a decrease of 2.5 kW (18.4 %) of the copper and iron losses in the rated operation point is achieved, as it can be seen in Figure 10. As an overall result, the efficiency of the VI-PMSM with improved rotor pole geometry is higher than that of the reference machine, mainly due to the significant reduction of the iron losses. In the rated operation point the efficiency is 98.51 % as opposed to 98.27 % (see Figures 11a and 11b).

Furthermore, as shown in Figure 11b, the improved VI-PMSM design displays a larger area with an efficiency of over 98.5 % (for lower speeds and higher torques) than the reference machine. This has a positive influence on the overall efficiency for defined operation cycles, especially for WT applications.

5. Conclusion

This paper proposes and illustrates the advantages of an alternative drive train with six high-speed generators as a viable application for a 6 MW WT. First, three electrical machines are outlined based on analytical calculations and the VI-PMSM is chosen as the most suited topology. An existent design is then up scaled to 1 MW, in order to meet the requirements of this specific application. The efficiency map of this reference design is then implemented into a simple model of the drive train in order to proof the validity of the suggested concept. It is shown that multiple generators can offer the possibility of an unsymmetrical power split of the input wind power, which yields an efficiency gain for partial load operation of almost 6 %.

Furthermore, a method to improve the operational behavior of the reference VI-PMSM design, based on sinusoidal rotor field poles, is introduced. An air gap ratio is defined as a design parameter of the different rotor shapes and used to compare the reference machine to an exemplary adapted geometry.

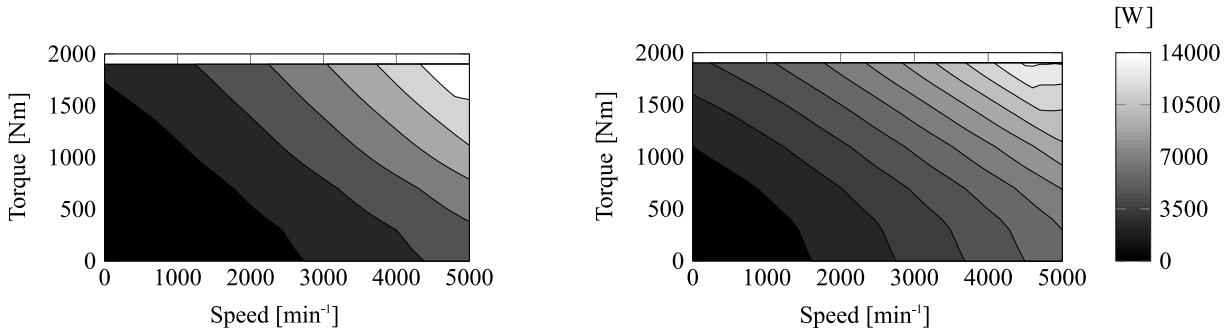

(a) $\frac{\delta_q}{\delta_d}$=1 (b) $\frac{\delta_q}{\delta_d}$=4

Fig. 10. Total losses for different $\frac{\delta_q}{\delta_d}$.

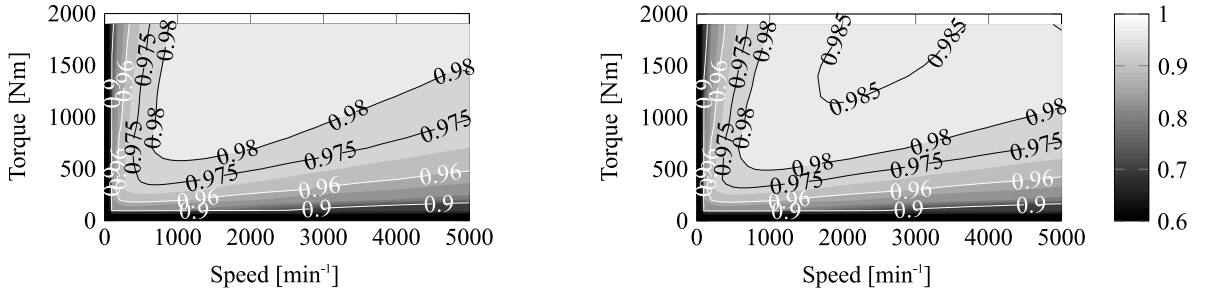

(a) $\frac{\delta_q}{\delta_d}$=1 (b) $\frac{\delta_q}{\delta_d}$=4

Fig. 11. Efficiency maps for different $\frac{\delta_q}{\delta_d}$.

Simulations show that a reduction of the cogging torque of almost 86 % and a reduction of the total losses of more than 18 % in the rated operation point are achieved, for a rotor geometry with an air gap ratio of $\frac{\delta_q}{\delta_d}$=4.

In future works, the other two electrical machine topologies regarded here—the SCIM and the EESM—will also be investigated in more detail, based on numerical simulations.

Especially the SCIM could turn out to be an interesting choice for this WT concept, due to the high efficiency and power density that result from this high-speed application. Moreover, the reduction of downtimes and maintenance costs for this WT configuration will also be regarded.

6. Acknowledgement

This work was funded by the German Federal Ministry for Economic Affairs and Energy under Grant 0325642.

References

1. Fried, L., Sawyer, S., Shukla, S., Qiao, L.: *Annual Market Update 2012*. Technical Report, Global Wind Energy Council GWEC, Brussels, 2013.
2. Newton, C.: *Trends in Electrical System Technology for Wind Turbines*. In: Proceedings of the European Wind Energy Conference & Exhibition EWEC 2006, February 27 – March 2, 2006, Athens, p. 1–7.
3. Cotrell, J.R.: *A Preliminary Evaluation of a Multiple-Generator Drive Train Configuration for Wind Turbines.* In: Proceedings of the 21st American Society of Mechanical Engineers ASME Wind Energy Symposium, January 14–17, 2002, Reno, p. 1–8.
4. Ribrant, J., Bertling, L.M.: *Survey of Failures in Wind Power Systems with Focus on Swedish Wind Power Plants during 1997–2005.* In: IEEE Transactions on Energy Conversion, XXII (2007), No.1, March 2007, p. 167–173.
5. Ribrant, J.: *Reliability performance and maintenance – a survey of failures in wind power systems.* Master Thesis, KTH School of Electrical Engineering, Stockholm, 2006.
6. Smolders, K., Long, H., Feng, Y., Tavner, P.J.: *Reliability Analysis and Prediction of Wind Turbine Gearboxes.* In: Proceedings of the European Wind Energy Conference & Exhibition EWEC 2010, April 20–23, 2010, Warsaw, p. 1–7.
7. Spinato, F., Tavner, P.J., van Bussel, G.J.W., Koutoulakos, E.: *Reliability of wind turbine subassemblies*. In: IET Renewable Power Generation, III (2009), No.4, 2009, p. 387–401.
8. Hansen, A.D., Iov, F., Blaabjerg, F., Hansen, L.H.: *Review of Contemporary Wind Turbine Concepts and their Market Penetration.* In: Wind Engineering, XXVIII (2004), No.3, 2004, p. 247–263.

9. Salles, M.B.C., Hameyer, K., Cardoso, J.R., Grilo, A.P., Rahmann, C.: *Crowbar System in Doubly Fed Induction Wind Generators.* In: Energies, III (2010), No.4, April 2010, p. 738–753.
10. Hau, E.: *Wind Turbines: Fundamentals, Technologies, Applications, Economics.* Springer, London, 2013.
11. Heier, S.: *Windkraftanlagen: Systemauslegung, Netzintegration und Regelung (Wind Energy Systems: System Design, Grid Integration and Control)*. Vieweg+Teubner, Wiesbaden, 2009.
12. Li, H., Chen, Z.: *Overview of different wind generator systems and their comparisons.* In: IET Renewable Power Generation, II (2008), No.2, June 2008, p. 123–138.
13. Polinder, H., van der Pijl, F.F.A., de Vilder, G.-J., Tavner, P.J.: *Comparison of Direct-Drive and Geared Generator Concepts for Wind Turbines.* In: IEEE Transactions on Energy Conversion, XXI (2006), No.3, September 2006, p. 725–733.
14. Achzet, B.: *Empirische Analyse von preis- und verfügbarkeitsbeeinflussenden Indikatoren unter Berücksichtigung der Kritikalität von Rohstoffen (Empirical Analysis of Indicators that Influence Price and Availability under Consideration of the Criticality of Raw Materials).* PhD Thesis, disserta, Hamburg, 2012.
15. Barthel, T., van Gelder, K., Zeichfüßl, R.: *Hybrid Drive 3.0 MW – Development and Testing of a New Drive Train Concept.* In: Proceedings of the 1st Conference for Wind Power Drives CWD 2013, March 19–20, 2013, Aachen, p. 215–234.
16. Prasai, A., Yim, J.-S., Divan, D., Bendre, A., Sul, S.-K., Kreikebaum, F.: *A New Architecture for Offshore Wind Farms.* In: IEEE Transactions on Power Electronics, XXIII (2008), No.3, 2008, p. 1198–1204.
17. Bywaters, G., John, V., Lynch, J., Mattila, P., Norton, G., Stowell, J., Salata, M., Labath, O., Chertok, A., Hablanian, D.: *Northern Power Systems WindPACT Drive Train Alternative Design Study Report.* Technical Report, National Renewable Energy Laboratory NREL, Colorado, October 2004.
18. Müller, G., Vogt, K., Ponick, B.: *Berechnung elektrischer Maschinen (Design of Electrical Machines).* Wiley-VCH, Weinheim, 2008.
19. Eggers, D., Steentjes, S., Hameyer, K.: *Advanced Iron-Loss Estimation for Nonlinear Material Behavior.* In: IEEE Transactions on Magnetics, XLVIII (2012), No.11, November 2012, p. 3021–3024.
20. Atallah, K., Howe, D., Mellor, P., Stone, D.: *Rotor Loss in Permanent-Magnet Brushless AC Machines.* In: IEEE Transactions on Industry Applications, XXXVI (2000), No.6, November 2000, p. 1612–1618.
21. Alexandrova, J., Jussila, H., Nerg, J., Pyrhönen, J.: *Comparison between Models for Eddy-Current Loss Calculations in Rotor Surface-Mounted Permanent Magnets*. In: Proceedings of the 19th International Conference on Electrical Machines ICEM 2010, September 6–8, 2010, Rome, p. 1–6.
22. Finken, T., Hombitzer, M., Hameyer, K.: *Study and Comparison of several Permanent-Magnet excited Rotor Types regarding their Applicability in Electric Vehicles*. In: Proceedings of the eMobility – Electrical Power Train VDE Conference, November 8–9, 2010, Leipzig, p. 1–7.
23. Richter, R.: *Elektrische Maschinen: Allgemeine Berechnungselemente (Electrical Machines: General Design Elements)*. Birkhäuser, Basel, 1951.
24. Andrei, C., Kauder, T., Karthaus, J., Hombitzer, M., Appunn, R., Hameyer, K.: *Improved Rotor Pole Geometry of a PMSM for Wind Turbine Applications with Multiple High-speed Generators.* In: Proceedings of the International Conference on Optimization of Electrical and Electronic Equipment (OPTIM), May 22–24, 2014, Brasov, p. 450–457.